Materials Advances

ROYAL SOCIETY OF CHEMISTRY

PAPER

View Article Online
View Journal | View Issue

Check for updates

Cite this: *Mater. Adv.*, 2024, 5, 741

Simple photocleavable indoline-based materials for surface wettability patterning†

Alex S. Loch, [a] Douglas Cameron, [b] Robert W. Martin, [b] Peter J. Skabara [a] and Dave J. Adams *[a]

There is a continued interest for smart surfaces that can transition between being hydrophobic or hydrophilic on-demand. Surfaces that can be switched with light are highly attractive, where the wettability properties of the surface or photopatterned water channels can be remotely controlled. However, many existing systems are complex, rely on synthetically challenging materials, lack reproducibility, or involve costly and intricate fabrication methods. Here, we introduce a straightforward approach using indoline-based, small molecules for the simple and precise control of a surface's wettability, using UV light as the external trigger. The wettability transition is accomplished through the photocleavage of the *o*-nitroanilide moieties, resulting in substantial water contact angle changes of up to 61°. Simplicity is achieved through solution-based spin-coating for material deposition, while each of the photoproducts were investigated using UV-vis and NMR studies, concluding that photocleave was fast and efficient (both in solution and the solid-state). Each material showed complete thermal stability within their operational range, while the best performing materials, **7-OH** and **9-OH**, produced smooth, high-quality coatings (RMS 0.24 and 0.50 nm, respectively). Furthermore, we demonstrated their use for wettability patterning and water channel creation, highlighting the materials suitability for integration in smart surfaces. This work offers an extremely accessible pathway to develop light-activated responsive surfaces.

Received 22nd November 2023,
Accepted 8th December 2023

DOI: 10.1039/d3ma01039b

rsc.li/materials-advances

Open Access Article. Published on 08 December 2023. Downloaded on 12/9/2025 2:58:29 AM.
This article is licensed under a Creative Commons Attribution 3.0 Unported Licence.

Introduction

On-demand wettability is an important aspect of designing and controlling smart surfaces. Surface coatings capable of transitioning between hydrophobic and hydrophilic states have applications in wettability patterning, biomolecular and biomedical contexts, debonding-on-demand, and sensing applications. As such, these devices can influence liquid behaviour, define channels, and produce self-cleaning surfaces and microfluidic systems.[1–3] While there are several ways in which a wettability switch can be achieved (*e.g.*, counter ion exchange, temperature, pH, electric current), the most non-invasive processes use light, which inherently allows for the 'stand-off' control of surface properties.[4,5] Due to this advantage, the development of surface coatings that can be switched or patterned using ultraviolet (UV) or visible light are of continued interest.

There are numerous examples of materials that photoswitch wettability through physical or chemical changes. Photoresponsive compounds, such as azobenzene,[4] spiropyran,[6] diarylethene,[7] and many others,[8,9] have been extensively studied for their ability to reversibly alter surface energy and/or physical geometry upon irradiation. While these reuseable materials have gained significant attention, they generally require extensive and costly synthetic and fabrication techniques, with an overall trend of minimal benefit compared to their complexity. Furthermore, these systems are highly susceptible to fatigue, leading to unexpected or rapid degradation of the desired switch.[10,11] Adding to their complexity, many of these materials are processed and tested as functionalised monolayers, emphasising minimal material consumption and chemical bonding to the substrate, as key advantages. However, to achieve reproduceable results, a functionalised monolayer requires a high-density loading of a linker group between the substrate and the material, in which a silane derivative such as (3-aminopropyl)triethoxysilane (APTES) is commonly employed. Although there is sufficient evidence that APTES (or other similar silane- or thiol-based monolayer linkers) must be prepared following precise steps to ensure both a high-density loading and to prevent multilayer and oligomer growth, many reports still use procedures that are ineffective, adding uncertainty and reducing repeatability in wettability patterning.[12–14] In particular, the application of APTES in anhydrous toluene solution (normally 1–10% loading) is continuously reported as a means of installing a monolayer linker moiety, yet under these conditions, multilayer growth occurs with no means of preventing or controlling the formation of two- and three-dimensional polymer chains. As surface wettability is influenced

[a] *School of Chemistry, University of Glasgow, G12 8QQ, UK. E-mail: dave.adams@glasgow.ac.uk*
[b] *Department of Physics, SUPA, University of Strathclyde, G4 0NG, UK*

† Electronic supplementary information (ESI) available. See DOI: https://doi.org/10.1039/d3ma01039b

© 2024 The Author(s). Published by the Royal Society of Chemistry

Open Access Article. Published on 08 December 2023. Downloaded on 12/9/2025 2:58:29 AM.
This article is licensed under a Creative Commons Attribution 3.0 Unported Licence.

by both the chemical structure and surface topography,[15] fabrication methods that offer consistency across batches and avoid variability, complexity, or lack redundancy are preferred.

Unlike reversible materials, photocleavable materials, though single use, can produce dependable devices that always perform as expected. While there are many organic materials that undergo photocleavage, the focus of this study was to use simple materials that can be easily processed into switchable surface coatings. As such, we identified that nitroaryl small molecules could be solution-processed and spin-coated for ease of fabrication and can be substituted to allow for photocleavage using UV light irradiation. *o*-Nitrobenzylic materials have been extensively used as photolabile groups in various applications, ranging from protecting groups to light-induced release systems and stimulus-responsive supramolecular scaffolds.[16–18] However, the rate of photoreaction is heavily dependent on the pH of the environment (for solution-based systems), and they are not suitable for applications where the rapid release of the photoproduct is required.[19] The use of *o*-nitrobenzyl ester materials has somewhat mitigated these rate-limiting challenges by providing a better leaving group (typically carbonic acid derivatives), although these materials still present issues of internal filtering from the formation of nitrosoaldehyde photoproducts.[18] Alternatively, *o*-nitroanilide materials are known to photocleave through an electrophilic *N*–*O*–acyl intermediate.[20–22] The reactivity of this intermediate, and therefore the efficiency of the photocleavage (up to 95% yield in solution)[23,24] has also enabled their use as protecting groups for a wide range of substituents.[25] Further work has demonstrated that substitution of the indoline ring can be used as a means of controlling the photoproduct or speed of the photocleavage, which in some cases completely prevents cleavage. Interestingly, the photocleavage of *o*-nitroanilides can be achieved in the solid state, without the need for additional stimulus (*i.e.*, solvent vapour atmosphere or washing/dipping the surface into a cleaning solution is not required), with the proposed mechanism shown in Fig. 1a.[22,26] Here, we use the photocleavage of three series of simple indoline-based materials for surface wettability patterning (Fig. 1b). The first series of materials incorporates a carbamide between the nitroindoline and side chain moiety. The use of *o*-nitroanilide carbamide materials has already been shown to produce acceptable cleavage yields (up to 65%) in the neat film.[22] The second series uses a carbamate linker, while the third explores the combination of a carbamate-phenyl linker. Each of the series contains two materials, one with a hydrophobic end group (*tert*-butyl ester) and the other with a hydrophilic end group (carboxylic acid). We describe the materials synthesis, physical and photophysical properties, and evaluate their use as simple surface coatings for wettability patterning.

Results and discussion

Synthesis

The synthetic pathway for each of the photocleavable materials is outlined in Fig. 2. A similar strategy was employed for each material. Firstly, indoline was protected with an acetyl group through reaction with acetyl chloride, affording **2** in a 94% yield. This allowed for double nitration at the 5- and 7-position of the protected material, leading to formation of **3** in a similar yield of 94%, although this contained approximately 2% of the singly substituted by-product (determined by NMR spectroscopy). Removal of the acetyl protecting group was completed under aqueous acidic conditions. Compound **4** was isolated in a 95% yield following recrystallisation, which also allowed for removal of the singly nitrated impurity. Addition of the acyl chloride functionality for coupling to each of the side chains was achieved using triphosgene, pyridine, and dichloromethane under anhydrous conditions, giving **5** as a yellow solid that was used immediately without purification.

Each of the *tert*-butyl ester end-capped materials were then prepared through either standard amide coupling to give **6-*t*Bu** or ester formation to give **8-*t*Bu** and **10-*t*Bu** in yields of 48%, 93%, and 66% respectively. Each of the materials were obtained as an amorphous powder. Final conversion to the corresponding carboxylic acid was achieved by stirring in a mixture of trifluoroacetic acid and dichloromethane. Subsequent removal of the solvent and excess trifluoroacetic acid gave

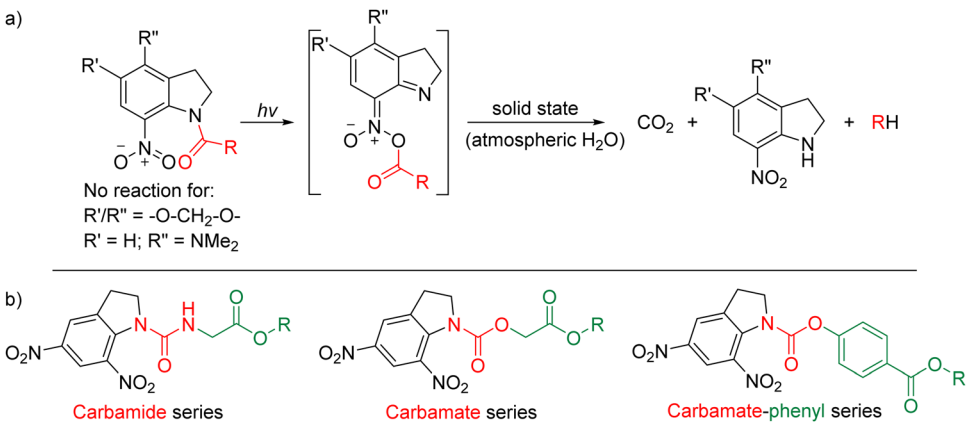

Fig. 1 (a) Schematic mechanism for the photocleavage of *o*-nitroanilide-based materials.[22] (b) The three series investigated in this study, where R = *tert*-butyl or H.

© 2024 The Author(s). Published by the Royal Society of Chemistry

Open Access Article. Published on 08 December 2023. Downloaded on 12/9/2025 2:58:29 AM.
This article is licensed under a Creative Commons Attribution 3.0 Unported Licence.

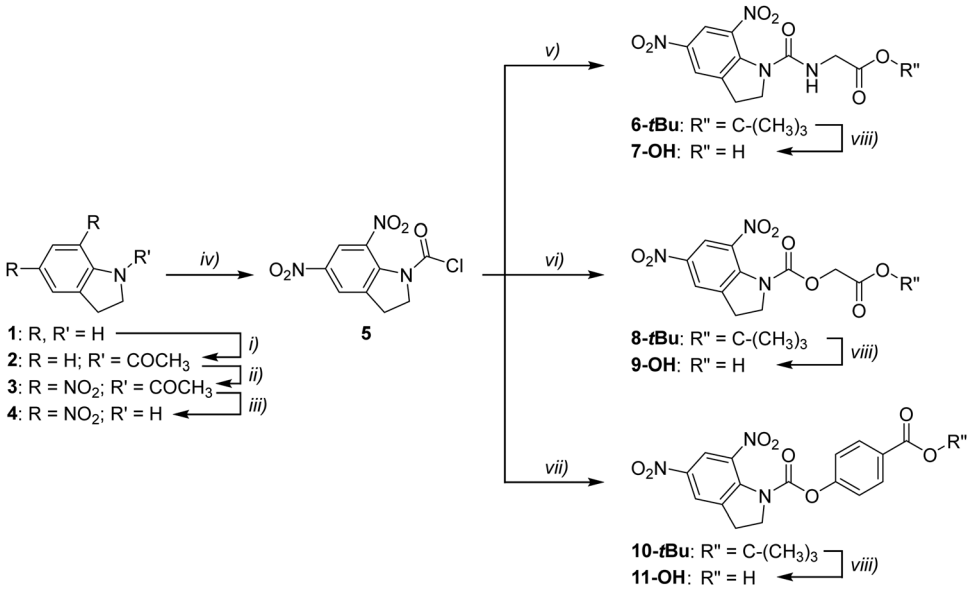

Fig. 2 Synthetic pathway to each of the photocleavable materials investigated in this study. Conditions and reagents: (i) acetyl chloride, acetic acid, 90 °C, 3 h; (ii) sodium nitrate, trifluoroacetic acid, O/N; (iii) hydrochloric acid (6 M, aq.), ethanol, reflux, 2 h; (iv) triphosgene, anhydrous pyridine, anhydrous dichloromethane, nitrogen atmosphere, 4 h; (v) glycine *tert*-butyl ester hydrochloride or (vi) *tert*-butyl 2-hydroxyacetate or (vii) *tert*-butyl 4-hydroxybenzoate, 4-(dimethylamino)pyridine, anhydrous dichloromethane, nitrogen atmosphere, O/N; (viii) trifluoroacetic acid, dichloromethane, 2 h.

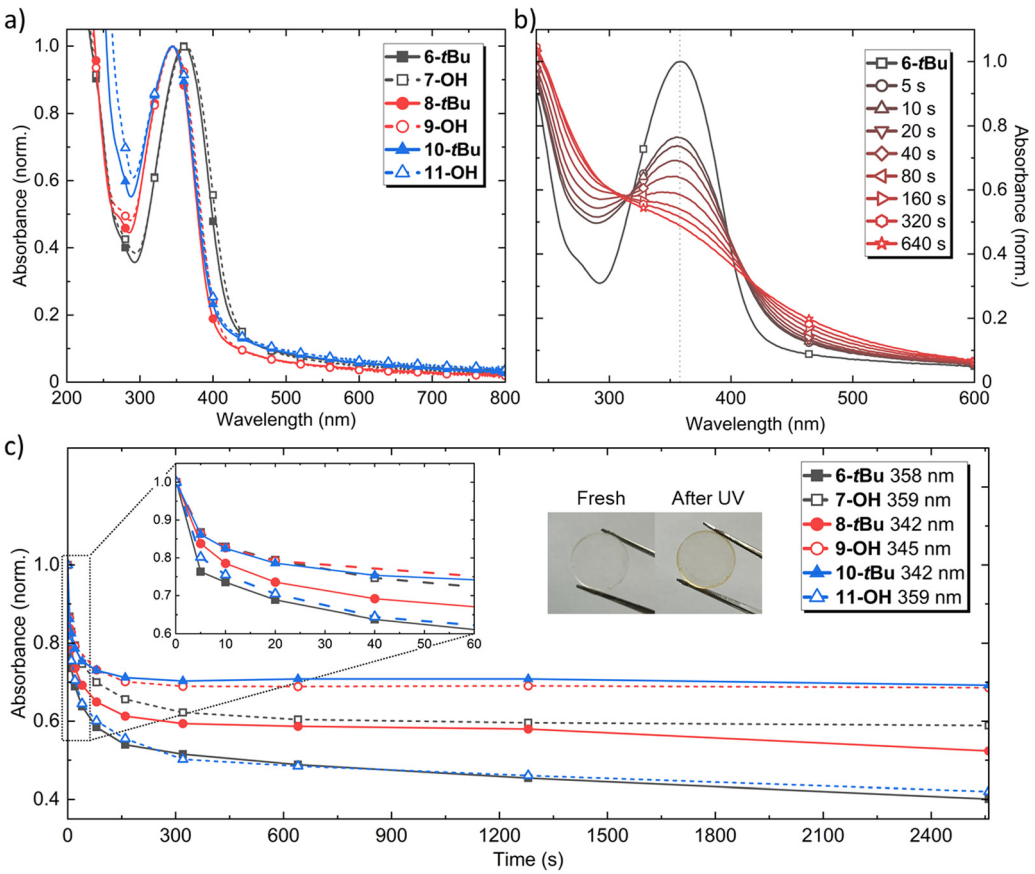

Fig. 3 (a) Neat film absorption of each of the materials. (b) Change in the UV-vis spectrum of **6-*t*Bu** upon irradiation by a 365 nm LED. (c) Change in the peak absorption of each material upon 365 nm LED irradiation. Insert: Picture of a neat film of **6-*t*Bu** before (left) and after (right) the irradiation experiment. The dashed vertical line in (b) represents the change plotted in (c). The LED power for all measurements was 161 mW cm^{-2}.

Open Access Article. Published on 08 December 2023. Downloaded on 12/9/2025 2:58:29 AM.
This article is licensed under a Creative Commons Attribution 3.0 Unported Licence.

7-OH, **9-OH**, and **11-OH** in yields of 96%, 93%, and 96%, respectively.

Optical properties

The UV-visible (UV-vis) absorption spectra of each of the materials were recorded in both solution (Fig. S1, ESI†) and thin film states (Fig. 3a). As anticipated, the absorption spectra of each material were similar between the solution and film, with each film measurement showing a tail of longer wavelength absorption attributed to intermolecular interchromophore interactions enabled by packing within the neat film. The two carbamide-based materials showed almost identical absorption and a slight red-shift compared to that of the carbamate series, which all showed a similar absorption peak around 345 nm. Due to the strong absorption of all materials from 300–400 nm, we used a 365 nm LED for irradiation to investigate the photocleavage and photoproducts. Photocleavage was evaluated in both tetrahydrofuran solution (Fig. S2 and S3, ESI†) and neat thin film (Fig. 3b, c and Fig. S5, ESI†). The solution results suggested bond-breakage was occurring between the indoline moiety and the side chain, as each spectrum shifted in good agreeance with the proposed photoproduct **4**. Photocleavage occurred extremely quickly, with significant intensity, peak shift, and shoulder feature changes seen after 5 seconds of irradiation. All of the materials exhibited a red shift of their peak absorption and appearance of a shoulder feature around 400 nm, consistent with the formation of **4**. All solutions showed a continual decrease in their absorption maximum with irradiation, except **9-OH**, which showed an increase to 1.4 after 40 seconds that then began to decay. We confirmed that **4** did not undergo any changes upon irradiation up to 320 seconds, after which a slight decrease in absorption was observed and attributed to photodegradation (Fig. S4, ESI†).

For the thin film measurements, an example of the change in the UV-vis spectrum of **6-*t*Bu** upon irradiation is shown in Fig. 3b, with the change in the peak absorption of each material shown in Fig. 3c (see General Experimental for neat film fabrication). All the materials followed a similar peak absorption decrease with irradiation, showing a rapid reduction ≈30% in the first 80 seconds that was accompanied by an increase in the tail absorption (>400 nm). None of the materials showed a peak-shift or the appearance of a defined shoulder feature like that observed with the solution results, however, the tail absorption increase gave rise to a colour change from transparent to yellow, as also seen with the solution results. A key finding was the speed of change upon irradiation. There was little difference in the peak absorption change in the first 5 seconds between the solution and film measurements, showcasing how efficiently the materials cleave even when processed into the solid-state. Overall, both the speed of photocleavage and the colour change (as a visual indicator) made them excellent candidates for photopatterning.

Photocleavage

We investigated the solution-based photocleavage product of each of the materials using NMR spectroscopy. Each of the *tert*-butyl ester end-capped materials (**6-*t*Bu**, **8-*t*Bu**, and **10-*t*Bu**) were

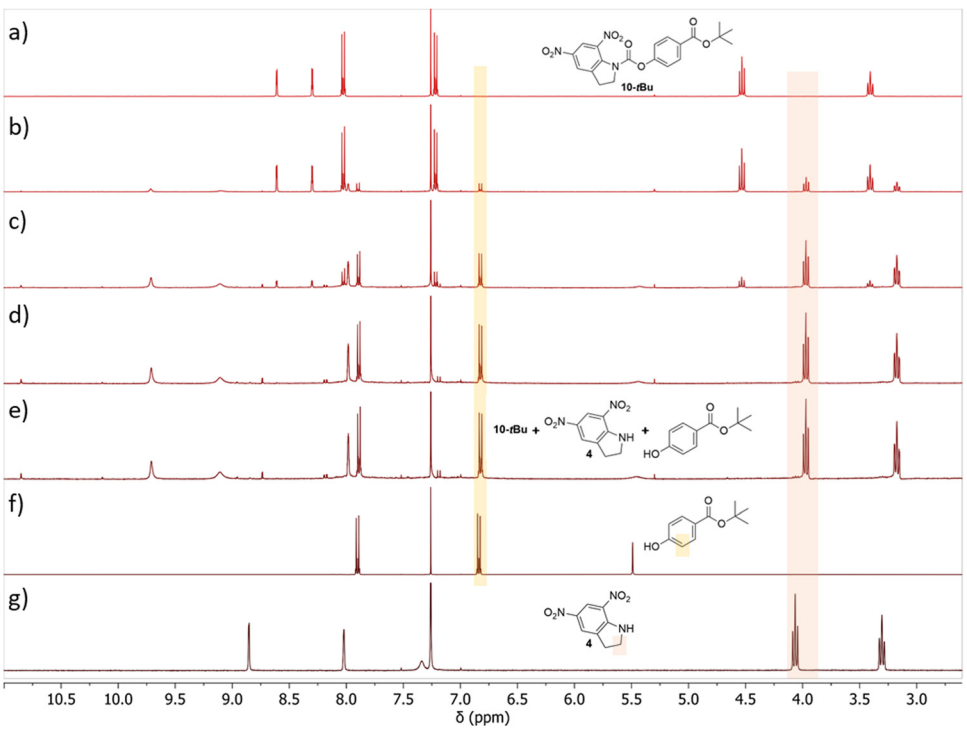

Fig. 4 Partial ^{1}H NMR (400 MHz, $CDCl_3$) spectra of (a)–(e) **10-*t*Bu** after irradiation for 0, 1, 5, 15, and 30 min by 2 × 365 nm LEDs (161 mW cm^{-2} each); (f) *tert*-butyl 4-hydroxybenzoate; and (g) **4**. The shaded areas across the spectra highlight the change in some key signal peaks of the proposed photoproduct.

© 2024 The Author(s). Published by the Royal Society of Chemistry

Open Access Article. Published on 08 December 2023. Downloaded on 12/9/2025 2:58:29 AM. This article is licensed under a Creative Commons Attribution 3.0 Unported Licence.

analysed in $CDCl_3$, while their corresponding carboxylic acids (**7-OH**, **9-OH**, and **11-OH**) were analysed in DMSO-d_6. It was expected that the two carbamides would cleave to give the free amine with a loss of carbon dioxide, while the carbamate materials would cleave to the terminal alcohol on the side chain group. As the concentrations in the NMR samples were significantly higher than that of the UV-vis experiments, we assessed any changes after longer irradiation times of 1, 5, 15, and 30 minutes, and doubled the flux by using two 365 nm LEDs faced towards the samples. An example of the changes observed for **10-*t*Bu** are shown in Fig. 4, while the other materials are shown in Fig. S6–S10 (ESI†). All materials showed signs of photodegradation through the appearance of multiple, minor by-products, however, the major photoproduct could be correlated to **4** through the loss of carbon dioxide, except in the case of **7-OH**. For most of the materials, we were also able to overlay the spectra of the expected side chain photoproduct, which agreed well as a mixture of both photoproducts. These results confirmed what was observed in the UV-vis experiments, that each of the materials respond rapidly and efficiently to photo-stimuli resulting in bond breakage.

Next, we tried to replicate these results after the materials had been processed into thin films by irradiating (as done previously) and then extracting the photoproducts with the NMR solvent. To increase the amount of available sample, thick films (15 mg mL^{-1}) were spin-coated onto larger, 15 × 15 mm glass substrates. However, in all cases, the signal-to-noise was too low to determine the major photoproducts (**7-OH** example Fig. S11, ESI†). It should be noted that **7-OH** and **11-OH** would not dissolve in concentrations above 20 mg mL^{-1}. A further attempt to investigate the changes of **7-OH** as a neat solid was attempted by finely crushing the powder in a glass dish before irradiating with two 365 nm LEDs (270 mW cm^{-2} each) for 4 hours. Although the solid and corresponding NMR solvent solution showed a distinct colour change, only minor changes were observed in the NMR spectrum (Fig. S12, ESI†). We concluded that only the outer of the solid was cleaved (and responsible for the colour change), which prevented light penetration into the bulk of the material. This issue was therefore not observed in the previous thin film studies and as this was how they were intended to be used, we were satisfied with the proposed photoproducts being formed from the solution and UV-vis experiments.

Thermal properties

As the materials were intended to be used as substrate coatings, we evaluated their thermal stability using thermal gravimetric analysis (TGA) and investigated if they underwent any thermal transitions during heating and cooling using differential scanning calorimetry (DSC), with the results summarised in Table 1. For the TGA measurements (Fig. S13, ESI†), the *tert*-butyl ester end-capped materials **8-*t*Bu** and **10-*t*Bu** showed an initial rapid mass loss ≈10%, which we attribute to the loss of an isobutylene moiety,[27] followed by thermal degradation. For **6-*t*Bu**, the observed decrease in weight was significantly more at ≈25%, which aligns well with the loss of both the isobutylene moiety and carbon dioxide.[22] This feature was not observed in the carbamate, carboxylic acid end-capped materials **9-OH** and **11-OH** (which only showed degradation), however **7-OH** also showed a loss ≈15%, which is again consistent with the loss of carbon dioxide. Overall, all materials were deemed thermally stable, showing no temperature-induced mass changes below 175 °C.

Next, DSC measurements were run from −20 °C to 200 °C over three cycles for each of the materials except **11-OH**, which was run from −20 °C to 290 °C (Fig. S14, ESI†). It was only possible to scan to a higher temperature with **11-OH** due to its higher thermal stability (to prevent contamination of the DSC instrument). **7-OH** and **11-OH** both showed the onset of a melting peak in the first heating cycle. However, the peak position could not be determined at scan rates of 10, 25, or 50 °C min^{-1}. No crystallisation transition was observed on the corresponding cooling cycle but a glass transition feature in the subsequent cycles was observed at 86 and 96 °C for **7-OH** and **11-OH**, respectively. **6-*t*Bu**, **9-OH**, and **10-*t*Bu** showed a complete melting peak in the first heating cycle followed by a glass transition feature on subsequent heating cycles. This is representative of an amorphous material, that upon melting, forms a glass on cooling which reveals the glass transition temperature (T_g) in following scans. **6-*t*Bu** only showed a partial crystallisation on the return cooling cycle, however we believe this was a consequence of being at the very end of the scan range. Interestingly, after the first heating cycle, **10-*t*Bu** showed smaller melting and crystallisation features on the subsequent heat–cool cycles. The un-uniform packing in the first cooling cycle was confirmed by the difference in the peak area (melt peak area = 85 J g^{-1}; crystallisation peak area = −39 J g^{-1}), with the appearance of the irregular melting and crystallisation features around 170 and 140 °C, respectively. **8-*t*Bu** showed two distinct melting peaks in the first heating scan, which is indicative of multiple polymorphs,[28] followed by a glass transition around 45 °C after removal of the material's thermal history. Knowing

Table 1 Summary of each material's thermal properties

	Mass change temperature (°C)	T_d (°C)	T_g (°C)	MP (°C)
6-*t*Bu	178 (–CO_2, –isobutylene; cal. 25%, found 27%), 205 (deg.)[a]	190	61	174
7-OH	185 (–CO_2; cal. 14%, found 12%), 205 (deg.)[a]	199	86	185
8-*t*Bu	179 (–isobutylene; cal. 15%, found 16%), 198 (deg.)[a]	186	45	146/177
9-OH	192 (deg.)[a]	223	46	188
10-*t*Bu	210 (–isobutylene; cal. 13%, found 12%), 231 (deg.)[a]	219	67	189
11-OH	267 (deg.)[a]	309	96	279[b]

[a] 'deg.' start of degradation. [b] Determined using a melting point apparatus and showed degradation.

Open Access Article. Published on 08 December 2023. Downloaded on 12/9/2025 2:58:29 AM.
This article is licensed under a Creative Commons Attribution 3.0 Unported Licence.

the melting point and glass transition temperatures of each of the materials, we used these results to probe if the surface wettability could be further manipulated by simple thermal annealing (see Surface Wettability below).

Surface wettability

To assess the effect of photocleavage on the surface characteristics, static contact angle measurements were conducted on each of the materials as neat films before and after 365 nm LED irradiation, with the results summarised in Table 2. Most interestingly, although all materials showed similar photocleavage behaviour in the UV-vis and NMR studies (speed and intensity of the change), only **7-OH** and **9-OH** showed significant contact angle changes of 52° and 55° after photocleavage, respectively. **8-*t*Bu** showed a smaller change of 18° when tested after minimal drying post-fabrication (1 h), however, this reduced to <10° after thorough film drying (overnight). **7-OH** and **9-OH** also showed differences in their measurements after complete drying, with **7-OH** increasing to a change of 61°, and **9-OH** decreasing to 45°. It was clear that the carboxylic acid end group functionality in **7-OH** and **9-OH** played an important role in having a hydrophilic surface pre-UV light irradiation, while the phenyl side chain group in **11-OH** prevented this. Additionally, each of the materials were thermally annealed at temperatures both above their T_g and melting point (determined in the previous Thermal Properties section, Table S1, ESI†). However, in all cases, the UV light-activated contact angle changes decreased to <40°, negating the possibility of further manipulating the surface coatings with heat.

To assess the useability of the materials for surface coatings, we performed some simple photopatterning experiments with fabricated films of **7-OH** and **9-OH**. An example of the change observed with a water droplet during static contact angle measurements is shown in Fig. 5a, and photopatterning experiments are shown in Fig. 5b and c. Firstly, we irradiated half a film of **9-OH** and assessed the change in surface characteristics on a single substrate. It was clear that photocleavage had occurred, resulting in an increase of the contact angle under the exposed region. As discussed previously, the exposed section of the films could also be identified visually, with a colour change from transparent to yellow/coloured (difference between left and right in Fig. 5b, separated by the dashed line).

Table 2 Static contact angle (°) measurements for each of the materials as a neat film before and after 365 nm LED irradiation (5 min at 161 mW cm^{-2}). The results are the average of a minimum of 4 measurements on a single film, with the given error as the standard deviation. Changes of <10° are not shown. 'As prepared' films were tested after 1 h of drying in a vacuum oven at 40 °C, while 'After drying' films were dried overnight

(°)	As prepared	After UV	Change	After drying	After UV	Change
6-*t*Bu	74 ± 1	73 ± 1	—	78 ± 1	79 ± 1	—
7-OH	30 ± 1	82 ± 1	52	20 ± 1	81 ± 1	61
8-*t*Bu	53 ± 1	71 ± 1	18	78 ± 1	81 ± 1	—
9-OH	23 ± 1	78 ± 1	55	28 ± 2	73 ± 1	45
10-*t*Bu	82 ± 1	79 ± 1	—	84 ± 1	84 ± 1	—
11-OH	79 ± 1	80 ± 2	—	76 ± 1	83 ± 1	—

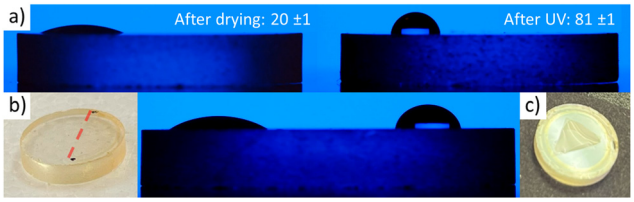

Fig. 5 (a) Example contact angle measurement of a thin film of **7-OH** before (left) and after (right) 365 nm LED irradiation. (b) Example of the contact angle change in a single film of **9-OH**, where half the film has been irradiated while the other half has been covered with a photomask. The red line in the picture (left) represents the location of the photomask, which gives rise to the change in the water droplet contact angle (right) on the same substrate. (c) Picture of how different photomasks can be used to control the surface wettability, herein a triangle shape photomask.

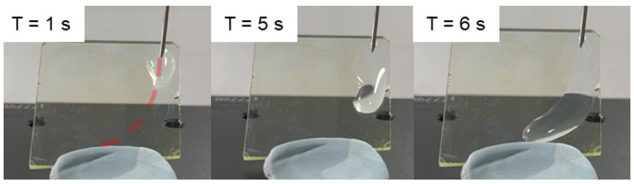

Fig. 6 Photographs of a patterned film of **7-OH** used to direct a water droplet. The dashed line represents the photomask pattern and expected direction of travel.

Simple patterns could also be transferred onto the substrates, like that observed in Fig. 5c, where the water droplet wells within the photopatterned triangle.

Additionally, **7-OH** was used as a surface coating for directing a water droplet along a defined path (Fig. 6). Thick films were spin coated on a microscope slide and a curved line photopatterned from the top right to the bottom middle (red dashed line) of the substrate. A water droplet was introduced *via* a syringe, which followed the designated path along the substrate before reaching the bottom. Not only did this validate the surface switching properties of the materials, but this was achieved without an intermediate washing and drying step (required by most photocleavage-based systems). Again, the simplicity of these materials allowed for light-mediated control over the surface wettability.

Surface topography

All of the films were examined using optical microscopy and cross-polarised optical microscopy (CPM) to assess if any changes could be viewed on a macroscopic level after photocleavage. All the materials produced good-quality, optically transparent films, which did not show any major features with or without cross-polarisation (Fig. S15, ESI†). After irradiation, only **9-OH** showed a significant change, with the introduction of pit-like features across the film's surface, although this did not translate in the CPM images (Fig. S16, ESI†). Overall, the optical microscopy images did not provide any insight into the observed changes in the static contact angle measurements.

For the best performing materials, **7-OH** and **9-OH**, we assessed the films topography using atomic force microscopy

© 2024 The Author(s). Published by the Royal Society of Chemistry

Open Access Article. Published on 08 December 2023. Downloaded on 12/9/2025 2:58:29 AM.
This article is licensed under a Creative Commons Attribution 3.0 Unported Licence.

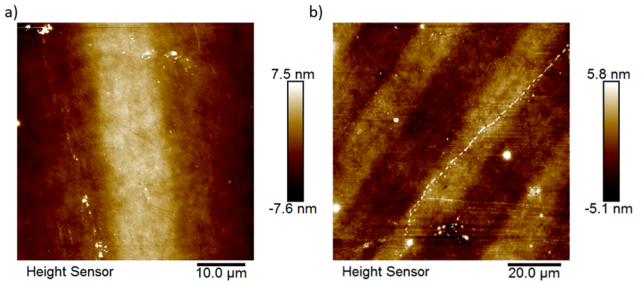

Fig. 7 (a) Small area and (b) larger area AFM topography image of a neat, thin film of **7-OH** after photopatterning. Note: The film was purposefully rotated between measurements.

(AFM). To accurately capture any changes that were induced by UV light irradiation, a repeating grid photomask (20 µm exposed, 14 µm no exposure) was used and the AFM tip scanned across the pattern, removing the need to lift the AFM tip between regions. For a thin film of **7-OH**, we firstly ran a large area scan over the film (Fig. 7b) confirming transfer of the photomask onto the film, although affected by a substrate defect (scratch). There is a clear definition between the exposed grid (darker contrast, negative height) and non-exposed grid (lighter contrast, positive height). Next, a smaller section was imaged, showing an overall height difference $\approx$7 nm between the exposed and non-exposed regions (Fig. 7a). The film showed no distinct patterns (outside of the photomask) or features and had an extremely low root-mean-square (RMS) roughness of 0.50 nm (ridge: 0.55 nm, valley: 0.44 nm). The static contact angle measurements across all the materials were very repeatable, which was again attributed to an extremely flat and smooth, good quality film. Unexpectedly, there were no features, changes, or grid pattern observed in the adhesion map (Fig. S17, ESI†). This suggests that there are no regions of favourable attraction between the film's surface and the AFM tip, yet a dramatic change is observed with a water droplet. The AFM topography results from a thin, neat film of **9-OH** mimicked that of **7-OH**, showing a height change $\approx$3 nm between exposed and non-exposed regions, with the addition of the pit-like features observed in the optical microscopy images (Fig. S18, ESI†), and a low RMS roughness of 0.24 nm (ridge: 0.30 nm, valley: 0.18 nm). However, unlike the microscopy images, they were uniform across the film, contradicting that they were a result of irradiation. The adhesion map also did not show any patterns, features, or changes between the exposed and non-exposed regions (Fig. S18c, ESI†). We concluded that the change in the contact angle is a consequence of switching of the chemical structure, from a more hydrophilic to a more hydrophobic surface, that occurs at the nanoscopic level.

Conclusion

We have showcased that simple materials and methodologies can be employed to control surface wettability. Using UV light as a trigger, the solid-state photocleavage of indoline, *o*-nitroanilide derivatives can be used to switch a surface from a more hydrophilic to hydrophobic state. We show the efficiency and simplicity of our system, where the coatings are deposited *via* spin coating, can be photopatterned quickly ($<$ 5 mins irradiation at 365 nm), and do not require additional washing or cleaning steps after pattern transfer. An additional benefit was a colour change (from transparent to yellow/coloured) upon irradiation, providing a visual indication of the patterned area or fluid channel. Both the side chain and end group played an important role in the material's ability to switch wettability, with minimal changes observed for the carbamate-phenyl side chain series and when using the hydrophobic *tert*-butyl end group. From this, the top-performing materials, **7-OH** and **9-OH**, both capped with a carboxylic acid end group, were found to switch a surface's water contact angle 61° and 45°, respectively. AFM measurements on neat, thin films of the two materials found them to be extremely smooth and flat, which provided reproducibility across the results. Transfer of a repeating grid photopattern was observed in the AFM height map, however, no features or changes were observed in the corresponding adhesion map. We concluded that surface wettability switching was due to nanoscopic changes to the materials' chemical structure and not a consequence of surface topography. Overall, these materials hold promise for a wide range of surface coating applications, especially where the precise, stand-off control of surface wettability is required.

Conflicts of interest

The authors declare no conflicts of interest.

Acknowledgements

This work was supported by the Engineering and Physical Sciences Research Council of the UK under the Hetero-print project (EP/R03480X/1).

Notes and references

1 S. Li, Y. Fan, Y. Liu, S. Niu, Z. Han and L. Ren, *J. Bionic. Eng.*, 2021, **18**, 473–500.
2 H. Liu, L. Zhang, J. Huang, J. Mao, Z. Chen, Q. Mao, M. Ge and Y. Lai, *Adv. Colloid Interface Sci.*, 2022, **300**, 102584.
3 L. Li, Z. Yan, M. Jin, X. You, S. Xie, Z. Liu, A. van den Berg, J. C. T. Eijkel and L. Shui, *ACS Appl. Mater. Interfaces*, 2019, **11**, 16934–16943.
4 C. Zong, M. Hu, U. Azhar, X. Chen, Y. Zhang, S. Zhang and C. Lu, *ACS Appl. Mater. Interfaces*, 2019, **11**, 25436–25444.
5 N. Wagner and P. Theato, *Polymer*, 2014, **55**, 3436–3453.
6 B. Yang, M. Lledos, R. Akhtar, G. Ciccone, L. Jiang, E. Russo, S. Rajput, C. Jin, M. G. F. Angelereou, T. Arnold, J. Rawle, M. Vassalli, M. Marlow, D. J. Adams and M. Zelzer, *Chem. Sci.*, 2021, **12**, 14260–14269.
7 S. Wandg, Y. Song and L. Jiang, *J. Photochem. Photobiol., C*, 2007, **8**, 18–29.

© 2024 The Author(s). Published by the Royal Society of Chemistry

Open Access Article. Published on 08 December 2023. Downloaded on 12/9/2025 2:58:29 AM.
This article is licensed under a Creative Commons Attribution 3.0 Unported Licence.

8 K.-Y. Chen, O. Ivashenko, G. T. Carroll, J. Robertus, J. C. M. Kistemaker, G. London, W. R. Browne, P. Rudolf and B. L. Feringa, *J. Am. Chem. Soc.*, 2014, **136**, 3219–3224.
9 N. B. Arndt, T. Adolphs, H. F. Arlinghaus, B. Heidrich and B. J. Ravoo, *Langmuir*, 2023, **39**, 5342–5351.
10 N. B. Arndt, F. Schlüter, M. Böckmann, T. Adolphs, H. F. Arlinghaus, N. L. Doltsinis and B. J. Ravoo, *Langmuir*, 2022, **38**, 735–742.
11 S. M. Varughese and N. Bhandaru, *Soft Matter*, 2020, **16**, 1692–1701.
12 A. R. Yadav, R. Sriram, J. A. Carter and B. L. Miller, *Mat. Sci. Eng., C*, 2014, **35**, 283–290.
13 S. S. Piletsky, A. Garcia Cruz, E. Piletska, S. A. Piletsky, E. O. Aboagye and A. C. Spivey, *Polymers*, 2022, **14**, 1595.
14 C. Vericat, M. E. Vela, G. Benitez, P. Carro and R. C. Salvarezza, *Chem. Soc. Rev.*, 2010, **39**, 1805.
15 W. Jiang, G. Wang, Y. He, X. Wang, Y. An, Y. Song and L. Jiang, *Chem. Commun.*, 2005, 3550.
16 C. Claaßen, M. H. Claaßen, F. Gohl, G. E. M. Tovar, K. Borchers and A. Southan, *Macromol. Biosci.*, 2018, **18**, 1800104.
17 Z. Tajmoradi, H. Roghani-Mamaqani and M. Salami-Kalajahi, *Polymer*, 2020, **205**, 122859.
18 P. Klán, T. Šolomek, C. G. Bochet, A. Blanc, R. Givens, M. Rubina, V. Popik, A. Kostikov and J. Wirz, *Chem. Rev.*, 2013, **113**, 119–191.
19 J. E. T. Corrie, A. Barth, V. R. N. Munasinghe, D. R. Trentham and M. C. Hutter, *J. Am. Chem. Soc.*, 2003, **125**, 8546–8554.
20 J. Morrison, P. Wan, J. E. T. Corrie and G. Papageorgiou, *Photochem. Photobiol. Sci.*, 2002, **1**, 960–969.
21 A. D. Cohen, C. Helgen, C. G. Bochet and J. P. Toscano, *Org. Lett.*, 2005, **7**, 2845–2848.
22 V. San Miguel, C. G. Bochet and A. del Campo, *J. Am. Chem. Soc.*, 2011, **133**, 5380–5388.
23 G. Papageorgiou and J. E. T. Corrie, *Tetrahedron*, 2000, **56**, 8197–8205.
24 B. Amit and A. Patchornik, *Tetrahedron Lett.*, 1973, **14**, 2205–2208.
25 S. Loudwig and M. Goeldner, *Tetrahedron Lett.*, 2001, **42**, 7957–7959.
26 A. A. Brown, O. Azzaroni and W. T. S. Huck, *Langmuir*, 2009, **25**, 1744–1749.
27 K. P. Cole, S. J. Ryan, J. M. Groh and R. D. Miller, *Bioorg. Med. Chem.*, 2017, **25**, 6209–6217.
28 W. Ishikawa, H. Inada, H. Nakano and Y. Shirota, *Chem. Lett.*, 1991, 1731–1734.

© 2024 The Author(s). Published by the Royal Society of Chemistry